# The X-Shooter Lens Survey - I. Dark-Matter Domination and a Salpeter-type IMF in a Massive Early-type Galaxy

C. Spiniello<sup>1\*</sup>, L.V.E. Koopmans<sup>1</sup>, S.C. Trager<sup>1</sup>, O. Czoske<sup>2</sup>, T. Treu<sup>3</sup>

- <sup>1</sup> Kapteyn Institute, University of Groningen, P.O. Box 800, 9700 AV Groningen, the Netherlands
- $^2$ Institut für Astronomie, Universität Wien, Türkenschanzstra $\beta$ e 17, 1180 Wien, Austria

24 August 2022

#### ABSTRACT

We present the first results from the X-shooter Lens Survey (XLENS): an analysis of the massive early-type galaxy SDSS J1148+1930 at redshift z = 0.444. We combine its extended kinematic profile – derived from spectra obtained with X-shooter on the ESO Very Large Telescope – with strong gravitational lensing and multi-color information derived from SDSS images. Our main results are (i) The luminosity-weighted stellar velocity dispersion is  $\langle \sigma_* \rangle (\lesssim R_{\rm eff}) = 351 \pm 10 \, {\rm km \, s^{-1}}$ , more accurate and considerably lower than a previously published value of  $\sim 450\,\mathrm{km\,s^{-1}}$ . (ii) A single-component (stellar plus dark) mass model of the lens galaxy yields a logarithmic total-density slope of  $\gamma' = 1.72^{+0.05}_{-0.06}$  (68 per cent CL;  $\rho_{\rm tot} \propto r^{-\gamma'}$ ). (iii) The projected stellar mass fraction, derived solely from the lensing and dynamical data, is  $f_*(< R_{\rm E}) = 0.19^{+0.04}_{-0.09}$  (68 per cent CL) inside the Einstein radius for a Hernquist profile and no anisotropy. The dark-matter fraction inside the effective radius  $f_{\rm DM}(< R_{\rm eff}) = 0.60^{+0.15}_{-0.06} \pm 0.1$  (68 per cent CL), where the latter error is systematic. (iv) Based on the SDSS colors, we find  $f_{*,Salp}(< R_E) = 0.17 \pm 0.06$  for a Salpeter IMF and  $f_{*,Chab}(< R_E) = 0.07 \pm 0.018$  for a Chabrier IMF. The lensing and dynamics constraints on the stellar mass fraction agree well with those independently derived from the SDSS colors for a Salpeter IMF, preferred over Chabrier. Dwarf-rich IMFs in the lower mass range of  $0.1-0.7 M_{\odot}$ , with  $\alpha \geqslant 3$  (with  $dN/dM \propto M^{-\alpha}$ ) – recently suggested by van Dokkum & Conroy for massive early-type galaxies – are excluded at the > 90 per cent C.L. and in some cases violate the total lensing-derived mass limit. We conclude that this very massive early-type galaxies is dark-matter dominated inside one effective radius, extending the trend recently found from massive SLACS galaxies, with a total density slope more shallow than isothermal. We exclude IMFs with  $\alpha = -3.5$  at the > 90 per cent CL, based on constraints set by lensing and dynamics.

 $\begin{tabular}{ll} \textbf{Key words:} & dark matter - galaxies: ellipticals - gravitational lensing: strong - galaxies: kinematics and dynamics - galaxies: structure - galaxies: formation \\ \end{tabular}$ 

#### 1 INTRODUCTION

Understanding the evolution and the internal structure of massive early-type galaxies (ETG), as well as their stellar and dark matter distributions, is crucial in order to fully comprehend the processes in hierarchical galaxy formation (e.g. White & Rees 1978; Davis et al. 1985; Frenk et al. 1985). In this context, the relationship between baryonic matter, that dominates astrophysical observables, and dark matter (DM), that dominates most of the dynamics during galaxy formation is particularly important.

\* E-mail: spiniello@astro.rug.nl

To unravel some of the these issues and paint a more robust physical picture, enormous effort has been afforded to study the relative contributions of baryonic, dark matter and black hole constituents of ETGs through stellar dynamical tracers, X-ray studies, and gravitational lensing (e.g. Fabbiano 1989; Mould et al. 1990; Saglia, Bertin & Stiavelli 1992; Bertin et al. 1994; Franx, van Gorkom & de Zeeuw 1994; Carollo et al. 1995; Arnaboldi et al. 1996; Rix et al. 1997; Matsushita et al. 1998; Loewenstein & White 1999; Gerhard et al. 2001; Seljak 2002; Borriello, Salucci & Danese 2003; Romanowsky et al. 2003, Treu & Koopmans 2004, Thomas et al. 2007, SAURON collaboration, Czoske

<sup>&</sup>lt;sup>3</sup>Department of Physics, University of California Santa Barbara, Santa Barbara, USA

et al. 2008, Czoske, Barnabé & 2008, Auger et al. 2010, Treu 2010).

The picture emerging over the last decades from studies of the inner regions of early-type galaxies, where baryonic and dark matter are both present, is that to first order the total mass density profile inside few effective radii can be well-described by a power-law form close to an isothermal profile with  $\gamma \approx 2$  for  $\rho_{\rm tot} = r^{-\gamma'}$ , although with a  $\sim 10$  per cent intrinsic scatter in the density profile (e.g. Gerhardt et al. 2001; Treu & Koopmans 2004; Koopmans et al. 2006, 2009; Auger et al. 2010, Barnabe et al. 2008, 2011). The dark-matter density profile in the same region, however, is far less well constrained although seems consistent with a density slope  $\gamma_{\rm DM} \approx 1.3$  (e.g. Treu & Koopmans 2004).

In addition, while the innermost regions of early-type galaxies are expected to be dominated by the stellar mass component, the dark-matter mass component is usually found to play a non-negligible role, with mass fractions ranging from 10 to 40 per cent of the total mass within one effective radius (e.g. Gerhard et al. 2001; Cappellari et al. 2006; Gavazzi et al. 2007; Weijmans et al. 2008). Even more recently, observations, as well as theoretical studies based on stellar population and dynamical models (e.g. Bullock et al. 2001, Padmanabhan et al. 2004), indicate that the dark matter fraction in the internal region increases monotonically with the mass of the galaxy (e.g. Zaritsky et al. 2006, Auger et al. 2010), a trend that is more conspicuous in the case of slow-rotator ellipticals (Tortora et al. 2009). On the other hand, it has also been shown that the luminous stellar mass-to-light ratio scales with the luminous mass of the system (Grillo et al 2010). However, information from stellar kinematics is limited to the central regions (a few effective radii) because of the lack of bright kinematic tracers at large radii, and the total mass determination suffers from the well-known degeneracy between the mass density profile of the galaxy and the anisotropy of its stellar velocity dispersion tensor (Binney & Mamon 1982). Higher-order velocity moments, which potentially allow one to disentangle this degeneracy by providing additional constraints (Gerhard 1993; van der Marel & Franx 1993), can only be measured with sufficient accuracy in the inner parts of nearby galaxies with current instruments. Despite great progress, it still remains difficult to separate the stellar and dark-matter components, mostly due to a still relatively poor understanding of the precise shape of the stellar IMF and its associated stellar mass-to-light ratio. Uncertainties related to the latter can easily lead to a factor of a few uncertainty in the inferred stellar mass.

Understanding the stellar IMF in massive early-type galaxies is a key open issue with a broad range of astrophysical implications. Although it is commonly assumed that the IMF is universal and independent of cosmic time, several authors have suggested that the IMF might indeed evolve (Dave 2008, van Dokkum 2008) or depend on the the stellar mass of the system (e.g. Treu et al. 2010; Graves & Faber 2010). Recently, van Dokkum & Conroy (2010) have suggested that low-mass stars ( $\lesssim 0.3\,M_\odot$ ) could be far more dominant in massive early-type galaxies than previously thought. This could imply that much of the increase in the mass-to-light ratio of galaxies with galaxy mass is due to a changing stellar IMF rather than an increasing dark-matter fraction.

Table 1. Properties of the cosmic Horseshoe.

	Parameter	Values
Lens	RA	11h 48m 33.15s
Galaxy	Dec	19° 30′ 03″5
	Redshift	0.444
	Effective radii (INT)	$1''.96 \pm 0''.02$
	Magnitude $g_L$	$(20.84 \pm 0.06) \text{ mag}$
	Magnitude $r_L$	$(19.00 \pm 0.02) \text{ mag}$
	Magnitude $i_L$	$(18.22 \pm 0.01) \text{ mag}$
	Magnitude $z_L$	$(17.75 \pm 0.04) \text{ mag}$
	Axis ratio (INT), $g$	$0.8 \pm 0.1$
Source	Redshift	$2.38115 \pm 0.00012$
	Star formation rate	$\sim 100  M_{\odot}  {\rm yr}^{-1}$
	Dynamical mass	$M_{vir} \simeq 10^{10} \ M_{\odot}$
Ring	Diameter	102
	Length	$\sim 300^{\circ}$
	Tot Magnitude $g, i$	21.6, 19.7  mag
	Mass enclosed	$(5.02 \pm 0.09) \times 10^{12} M_{\odot}$

<sup>&</sup>lt;sup>1</sup> Belokurov et al. (2007) measured the redshift of the source to be z=2.379. We find a systematic shift that brings the source redshift to be z=2.3811 in agreement with Quider et al. (2009).

Valuable additional information on distant early-type galaxies, besides their kinematics, can be provided by gravitational lensing. Strong gravitational lensing provides a very useful tool to investigate the total mass content of the lens (Maoz & Rix 1993, Rusin & Ma 2001; Rusin & Kochanek 2005; Dye & Warren 2005; Brewer & Lewis 2006b, 2008) and to place constraints on the inner mass distribution of lens galaxies at redshift out to  $z\simeq 1$ . Unfortunately, the mass-sheet and the related mass-profile (Wucknitz 2002) degeneracies do not always allow one to accurately determine the slope of the galaxy density profile and above all to unambiguously disentangle the luminous and dark matter components.

Gravitational lensing and stellar dynamics are particularly effective to break many of these degeneracies, when they are applied in combination in the analysis of the internal structure of distant early-type galaxies. The two approaches are complementary and allow, when combined self-consistently, to robustly determine the mass profile of the lens galaxy (Koopmans & Treu 2002, 2003, Treu & Koopmans 2002, 2003, 2004, Jiang & Kochanek 2007, Barnabé & Koopmans 2007, Czoske et al. 2008, Czoske, Barnabé & 2008, Koopmans et al. 2009, Grillo et al. 2010, Treu 2010, Barnabé et al. 2011). Disentangling stellar and dark matter remains difficult, but the uncertainties have been reduced from factors of a few to far less than this (Treu et al. 2010).

The X-shooter Lens Survey (XLENS) aim to take the next step and spectroscopically observe a sample of lens galaxies from the Sloan Lens ACS Survey (SLACS, Bolton et al. 2006) with  $\sigma_{\rm ETG} \geqslant 250 \, {\rm km \, s^{-1}}$  using the X-Shooter instrument<sup>1</sup>. With this data we intend to further disentangle

<sup>&</sup>lt;sup>2</sup> The mass within the Einstein radius or, more precisely, the ring diameter is taken from Dye et al. (2008).

<sup>&</sup>lt;sup>3</sup> Magnitudes are taken from SDSS D7

 $<sup>^1</sup>$  X-shooter is a powerful broad-band (3000–25000 Å), three-armed medium-resolution spectrograph on the VLT (D'Odorico

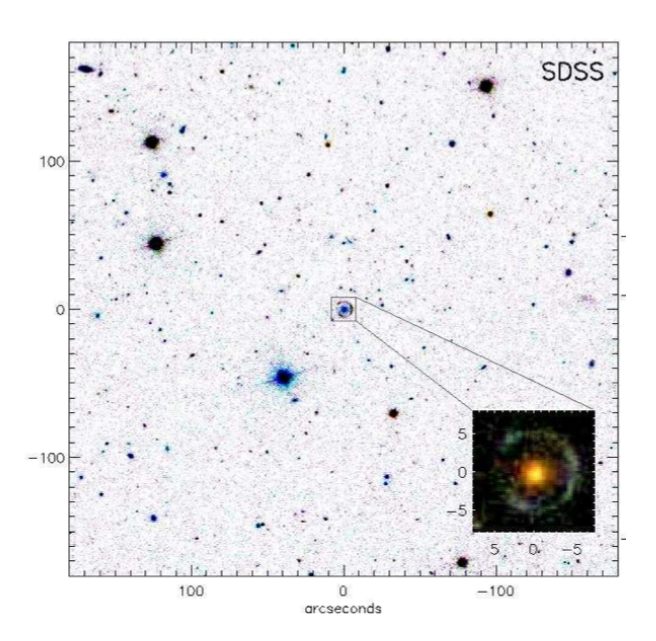


Figure 1. SDSS color composite image of the sky region around the Cosmic Horseshoe (the zoom is  $16'' \times 16''$ ).

the stellar and dark-matter content of the galaxies, through combined lensing, dynamical and *spectroscopic* stellar population studies. With multi-band HST images in hand, we are able to obtain more precise dark-matter mass fractions than ever before, in order to ultimately correlate these with ETG mass and compare with theoretical galaxy formation models. By combining the lensing and dynamical results with stellar population models we will plan to constrain the normalization and shape of the stellar initial mass function.

In this paper we present the result of a pilot program of the XLENS project: A study of the "Comic Horseshoe" (SDSSJ1148+1930), an almost complete Einstein ring with a diameter of  $\sim 10\rlap.{''}2$  around a very massive early-type galaxy at z=0.444. The system was discovered by Belokurov et al. (2007) in the Sloan Digital Sky Survey Data Release 5 (DR5). The source is a star-forming galaxy at z=2.381 (Dye et al. 2008, Quider et al, 2009). Properties and characteristics of the Cosmic Horseshoe are listed in Table 1 and a composite SDSS image of the system is shown in Figure 1.

The paper is organized as follows: In Section 2, we present the observations and data reduction. In Section 3, we discuss our kinematic analysis. In Section 4, we discuss the luminous and dark matter distributions of the lens galaxy. We summarize our findings and we present our conclusions in Section 5. We assume  $H_0 = 70\,\mathrm{km\,s^{-1}\,Mpc^{-1}}$ ,  $\Omega_\mathrm{m} = 0.3$  and  $\Omega_\Lambda = 0.7$  throughout the paper.

### 2 OBSERVATIONS AND DATA REDUCTION

X-shooter observations of SDSSJ1148+1930 were carried out during a GTO run between 17-24 March 2010 in slit

et al. 2006);  $22^h$  GTO time on three systems (084.A-0289 and 087.A-0620) and  $40^h$  GO time were awarded (P086.A-0312) to the XLENS project (PI: Koopmans)

Table 2. Observational details of the Cosmic Horseshoe

OB	Date	Exp. time (sec)	Seeing
200200337	3-17-2010	3 x 821(UVB - VIS)	062
		$3 \times 3 \times 274(NIR)$	
200200343	3-17-2010	3 x 821(UVB - VIS)	056
		$3 \times 3 \times 274(NIR)$	
200200436	3-19-2010	3 x 821(UVB - VIS)	0.466
		3 x 3 x 274(NIR)	

mode<sup>2</sup>, splitting the beam over three arms: UVB (R=3300 with 1".6 slit); VIS (R=5400, with 1".5 slit); and NIR (R=3300 with 1".5 slit), covering a wide wavelength range from 3000 to 25000Å simultaneously. The 11" long slit was centered on the galaxy with a position angle (PA) of 163°. The latter minimizes contamination from the source and leaves enough sky region to facilitate accurate sky subtraction. Two OBs were not used because of bad seeing and/or an incorrect positioning of the slit on the object. The total exposure time on target for each arm is  $\sim$  7389 sec and the typical seeing is  $\sim$  0".6. Standard calibration frames were obtained during daytime after the corresponding OB. A summary of the observing blocks is given in Table 2.

Data reduction was done using the ESO X-shooter pipeline, v1.2.1 (Goldoni et al. 2006), and the Gasgano data file organiser developed by ESO. The pipeline reduction uses calibration spectra, taken during the commissioning run, for bias subtraction and flat-fielding of the raw spectra. Cosmic rays are removed using LACosmic (van Dokkum 2001). For each arm, the orders are extracted and rectified in wavelength space using a wavelength solution previously obtained from the calibration frames. The resulting rectified orders are shifted and coadded to obtain the final two-dimensional (2D) spectrum. We extract a one dimensional spectrum (1D) from the resulting 2D merged spectrum, using an IDL code that makes use of the optimal-extraction algorithm of Horne (1986). It also produces the corresponding error file and bad pixel map. The final signal-to-noise ratio in the UVB+VIS spectrum is  $\sim 7$  per pixel. No telluric correction was applied. so that prominent atmospheric absorption bands can still be seen in the final spectrum (Fig 2).

Because the near-infrared spectrum suffers seriously from sky-line residuals using the current pipeline, we limit our analysis to the UVB-VIS region of the spectrum and defer a full analysis of the infrared data as well as our spectroscopic stellar-population analysis to future work. In this paper, we base our stellar mass determinations solely on the broad-band colors from the SDSS plus the stellar kinematic and lensing data.

# 3 STELLAR KINEMATICS

We measure the luminosity-weighted velocity dispersion of the lens galaxy from the final 1D UVB–VIS spectrum, using the Penalized Pixel Fitting (PPxF) code of Cappellari & Emsellem (2004). PPxF determines the combination of stellar templates which, when convolved with an appropriate line-of-sight-velocity distribution, best reproduces the galaxy spectrum. The best-fitting parameters of the LOSVD

 $<sup>^2</sup>$  P084.A-0289(A); PI: Koopmans

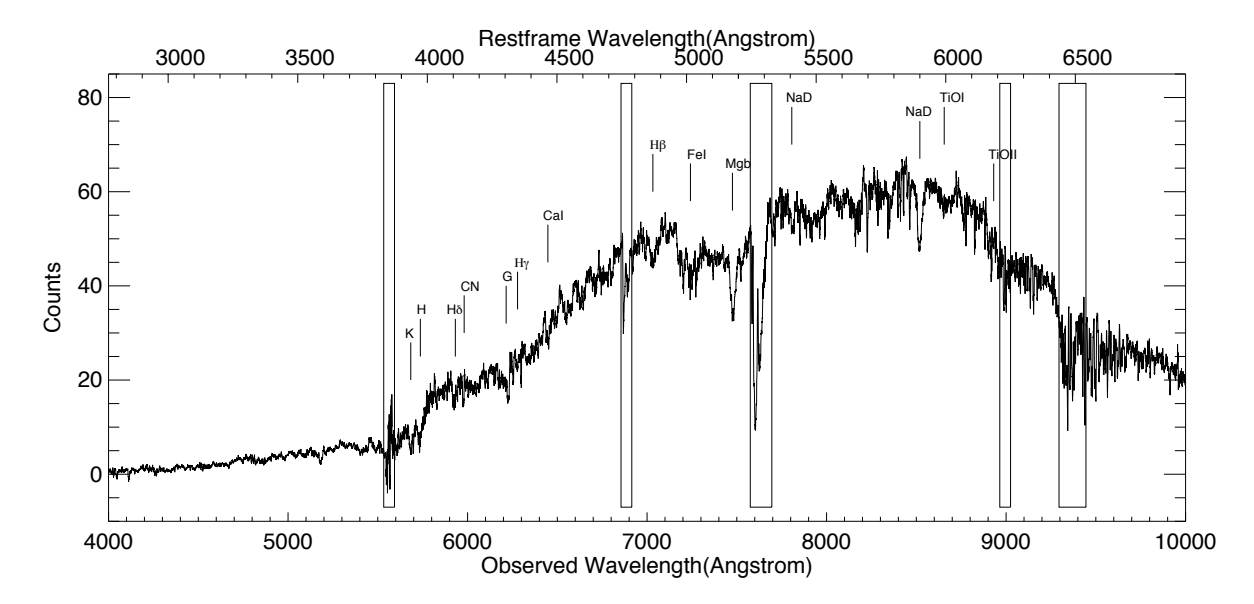


Figure 2. The final luminosity-weighted UVB-VIS 1D X-shooter spectrum extracted from a rectangular aperture of  $1.78 \times 1.76$  centered on the galaxy (see text). Spectral features the lens galaxy are marked. Telluric absorption lines have not been removed from the spectra. The boxes indicate parts of spectra that are affected by sky-lines order matching of spectral orders.

are determined by minimizing a  $\chi^2$  penalty function. The best fit provides the mean velocity and the velocity dispersion (v and  $\sigma$ , respectively), plus their error determination. The S/N ratio of the data is not adequate to measure the higher order Gauss-Hermite moments  $h_3$  and  $h_4$ , which quantify the asymmetric and symmetric departures of the LOSVD from a pure Gaussian (related to the skewness and kurtosis respectively). PPxF also allows the user to mask noisy or bad regions of the galaxy spectrum. We also perform an iterative sigma clipping in order to clean the spectrum of residual bad pixels, sky lines and cosmic rays.

We focus on absorption lines between 3500–5500Å (including Ca K and H, G4300,  $H_{\beta}$ ,  $Mg_{b}$  and some Fe lines). To minimize errors due to mismatch between templates and the galaxy spectra resolution, we use X-shooter stellar spectra obtained as part of the X-shooter Stellar Library (XSL) survey (Trager et al. 2011 in prep.), with same instrumental resolution ( $\sigma_{\rm instr} \sim 40\,{\rm km\,s^{-1}}$ ). An excellent fit is obtained with a weighted linear combination of a K1 giant template (57 per cent) and a G2 star template (43 per cent). The selected region (1...5) of our galaxy spectrum used for the fit and the corresponding best fit stellar template are shown in Figure 3.

# 3.1 Luminosity-Weighted Kinematics

The measured luminosity-weighted velocity dispersion<sup>3</sup> for the central aperture of 1".8×1".6 is  $\langle \sigma \rangle = 351 \pm 10 \pm 16 \, \mathrm{km \, s^{-1}}$ .

The formal error on the dispersion includes both the random error contribution and the systematic uncertainties due to spectral range differences, template mismatch and continuum fitting as discussed below. Figure 3 shows the best fitting template of the PPxF routine superimposed on the galaxy spectrum as well as the residuals of the fit.

As a first test of the accuracy of our measurements, we use the more heterogeneous MILES<sup>4</sup> stellar template library (Sánchez-Blázquez, et al., 2006). We select 100 stars (F, G, K, M) in the range 3525–7500Å, with 2.3Å FWHM spectral resolution. The measured luminosity-weighted stellar velocity dispersion of  $\langle \sigma \rangle = 358 \pm 31 \, \mathrm{km \, s^{-1}}$ , after instrumental correction, is consistent with the above estimate, based on XSL templates, but has larger errors due to the lower resolution of the MILES library. As a second test, we fit templates to two different spectral regions. We find slightly different results between the blue and the red part of the spectrum, but always consistent within  $2\sigma$  (not including systematics). The scatter in these fits is used to estimate additional systematic uncertainties related to template mismatches and spectra coverage.

# 3.2 Spatially-Resolved Kinematics

To preserve the spatially-resolved kinematic information, we define seven spatially-varying apertures (with adequate S/N ratio) along the radial direction and we sum the signal within each aperture. Apertures are defined to be larger than the seeing, in order to have independent kinematics measurements for each aperture. The stellar rotation velocity and velocity dispersion are measured in each aperture using PPxF,

 $<sup>^3</sup>$  The only velocity dispersion value previously published for the Cosmic Horseshoe is from Belokurov et al. (2007). They perform fits of Gaussian line profiles to the Ca H and K absorption lines from a much lower resolution spectrum (FWHM $\sim 10\mbox{\normalfont\AA}$ ). They find a higher velocity dispersion estimation of  $430\pm50\,\mbox{km}\,\mbox{s}^{-1}$ , inconsistent with our high-quality data.

 $<sup>^4\,</sup>$  http://www.iac.es/proyecto/miles/pages/stellar-libraries/miles-library.php

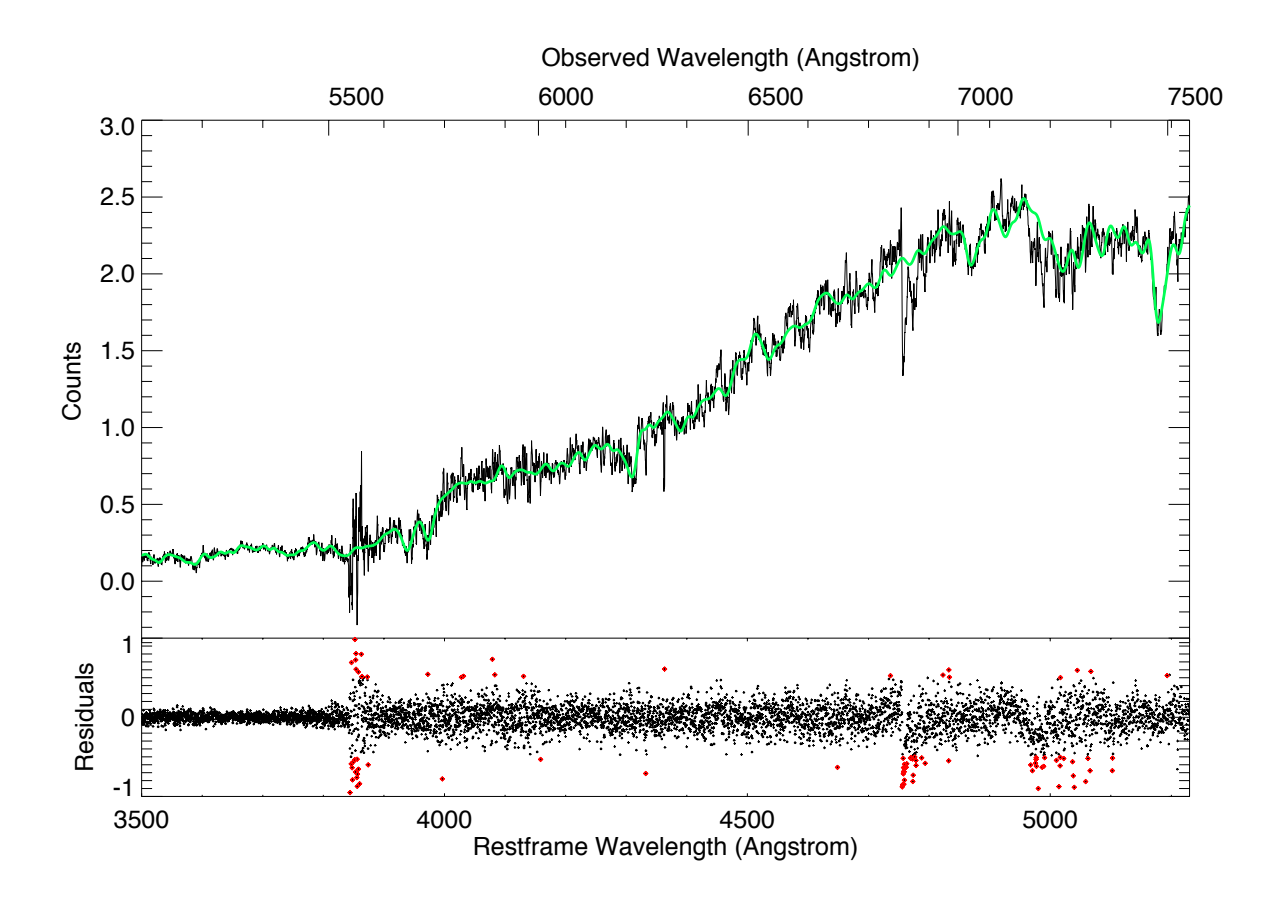


Figure 3. Top panel: Logarithmically rebinned UVB+VIS galaxy spectrum (black) and logarithmically rebinned best-fit template (green), both in restframe wavelength. Bottom panel: Residuals from the fit. Bad-pixels excluded from the fitting procedure (sky line, telluric lines) are shown in red. See the text for more information.

as described above. Again, we use different spectral regions, excluding the most prominent telluric lines in the VIS range and a range of seven XSL stellar templates (G, K and M stars). The uncertainties on the inferred kinematics are estimated by adding in quadrature the formal uncertainty given by PPxF and the scatter in the results for different templates and spectral regions. Details of the aperture sizes and the kinematic profiles are listed in Table 3. The rotation and the velocity dispersion profiles are shown is Figure 4.

We find an almost flat velocity dispersion profile beyond the effective radius. The weighted average value of  $344\pm25\,\mathrm{km\,s^{-1}}$  is consistent within the formal error with the luminosity weighted value for an aperture of  $1.8''\times1.6''$  (see Table 3), as expected. The velocity profile shows some mild rotation, with a projected rotation velocity of  $\sim140\,\mathrm{km\,s^{-1}}$  at one effective radius. Because the effective dispersion  $(v_{\rm rms}^2=\sqrt{v^2+\sigma^2};$  see Cappellari 2008) is well within the errors on  $\sigma$ , the effect of rotation can be neglected in our spherical Jeans analysis and we will ignore rotation in the remainder of this paper.

# 4 STELLAR AND DARK-MATTER

Here we derive the slope of the total density profile and calculate the fraction of dark matter inside one effective radius.

# 4.1 The Galaxy Mass Model

To derive the stellar mass inside the Einstein radius, we follow Treu & Koopmans (2002), Koopmans & Treu (2003), Treu & Koopmans (2004). We model the mass distribution as a superposition of the stellar and the dark matter components. For the stellar mass distribution we use two different spherical models, described by the equation:

$$\rho_*(r) = \frac{M_* r_*}{2\pi r^n (r + r_*)^{4-n}} \tag{1}$$

The Hernquist (1990) luminosity-density profile has n=1, and the Jaffe (1983) luminosity-density profile has n=2. The total stellar mass is  $M_*$  and the break-radius is  $r_*$ .

We model the dark matter distribution as a generalized spherical NFW profile, using a break radius of  $r_b = 50\,\mathrm{kpc}$  that is typical for massive ETGs although the result is insensitive to its exact value, and an outer slope of  $\gamma_{\mathrm{out}} = 3$ 

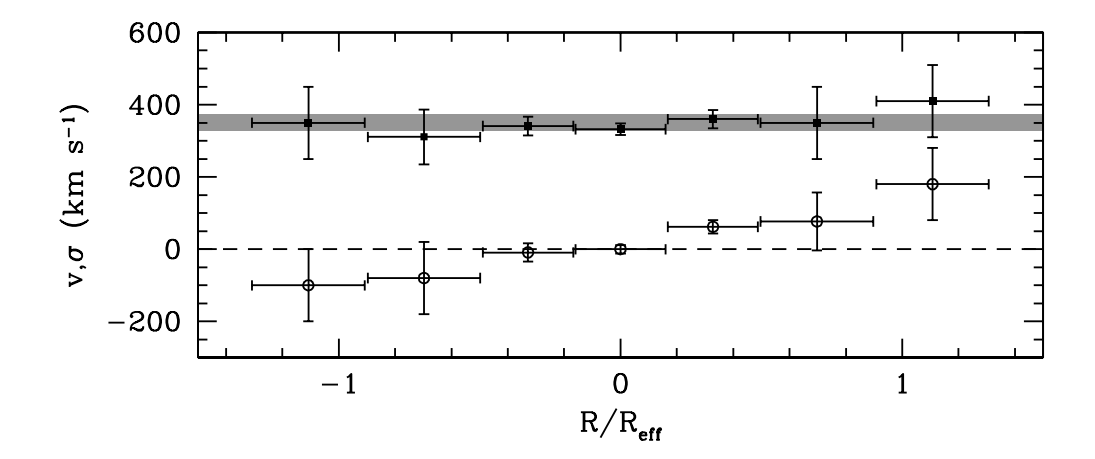


Figure 4. Kinematic profiles of the Cosmic Horseshoe. Rotation (bottom) and velocity dispersion (top). Grey line shows the light-weighted value for the central aperture.

(Gavazzi et al. 2007; Auger et al. 2010b), following the prediction from numerical simulations of dark matter halos (Ghigna et al., 2000):

$$\rho_{\rm DM}(r) = \frac{\rho_{d,0}}{(r/r_b)^{-\gamma} [1 + (r/r_b)^2]^{(\gamma - 3)/2}}$$
(2)

The break radius and the density scale  $(\rho_{d,0})$  determine the virial mass of the dark matter halo (Bullock et al., 2001).

For completeness, we also use a single mass component model where the stellar and dark-matter mass densities add to a power-law with an effective density slope  $\gamma'$  for  $\rho_{\rm tot} \propto r^{-\gamma'}$  and the stars are treated as trace particles (see Koopmans & Treu 2003).

The most accurately known constraint from the lens mass model is the mass inside the Einstein radius. We use  $M_{\rm E}=(5.02\pm0.09)\times10^{12}\,M_{\odot}$  inside  $\theta_{\rm E}=5\rlap.{''}1$  derived by Dye et al. (2008). The two (or single) mass components must add to  $M_{\rm E}$  within the Einstein radius. The error in radius is folded into the error in mass so that a fixed radius can be used (the mass and Einstein radius are coupled in the modeling). We use the average of the two effective radii from the g and i band images reported in Belokurov et al. (2007),  $R_{\rm eff}=1.96\pm0.02\,{\rm arcsec}$  (Table 1). The effective radius is uniquely related to  $r_*$  (see Hernquist 1983 and Jaffe 1990).

We also assume a constant orbital anisotropy parameter  $\beta$  and allow it to range between 0.0 and 0.5, which is typical for massive early-type galaxies (e.g. Gerhard et al. 2001). The parameters of the model without a strong prior are then the stellar mass  $(M_*)$  and the dark-matter density slope  $(\gamma)$ , or only  $\gamma'$  for the single-component model.

We subsequently solve the spherical Jean equations and compare the models to the kinematic data, taking the aperture sizes and seeing into account. We find an effective density slope of

$$\gamma' = 1.72^{+0.05}_{-0.06}$$
 (68percent C.L.)

when marginalizing over  $\beta=0.0$ –0.5, shallower than isothermal (see Koopmans et al. 2006 and 2009). This slightly low value for the logarithmic total-density slope may suggest that this object can be a group, or a small cluster of galaxies, where the overall efficiency of converting gas into stars is

Table 3. Spatially resolved kinematics of the Cosmic Horseshoe.

Aperture	Aperture	v	$\sigma$
center $('')$	$\mathbf{dimension}('')$	$({\rm km}{\rm s}^{-1})$	$({\rm km}{\rm s}^{-1})$
0.00, 0.00	$1.80 \times 1.60$	$0 \pm 15$	$351 \pm 10$
-2.16, 0.00	$0.80 \times 1.60$	$-100 \pm 100$	$350 \pm 100$
-1.36, 0.00	$0.80 \times 1.60$	$-80 \pm 100$	$311 \pm 76$
-0.64, 0.00	$0.64 \times 1.60$	$-9 \pm 25$	$341 \pm 26$
0.00, 0.00	$0.64 \times 1.60$	$0 \pm 12$	$332 \pm 16$
+0.64, 0.00	$0.64 \times 1.60$	$62 \pm 18$	$360 \pm 25$
+1.36, 0.00	$0.80 \times 1.60$	$77 \pm 80$	$350 \pm 100$
+2.16, 0.00	$0.80 \times 1.60$	$180\pm100$	$410\pm100$

lower. Changing the luminosity-density profile also does not change the final logarithmic slope significantly. The more interesting case of the two component model will now be discussed.

# 4.2 The Stellar Mass Fraction from Lensing and Kinematic Constraints

To derive the stellar mass fraction inside the Einstein radius, we create a densely sampled grid of likelihood values by comparing the kinematic profiles to the data for a projected stellar mass fraction  $[f^*(< R_{\rm E})]$  within the Einstein radius ranging between 0 and 1 and a dark-matter density slope  $(\gamma)$  ranging between 0.0 and 2.0. We assume flat priors on both quantities and marginalize over  $\gamma$  to derive the probability density function of  $f^*(< R_{\rm E})$ . The results for the Hernquist and Jaffe profiles are shown in Figure 5 for  $\beta=0$  and a more extreme case of radial anisotropy with  $\beta=0.5$ .

We find a fraction of stellar mass within the Einstein radius for the two luminosity profiles of:

$$f_{\text{HQ}}^* = 0.19_{-0.09}^{+0.04} \text{ and } f_{\text{JF}}^* = 0.13_{-0.05}^{+0.03} \text{ for } \beta = 0$$

and

$$f_{\rm HQ}^* = 0.13_{-0.07}^{+0.04}$$
 and  $f_{\rm JF}^* = 0.11_{-0.05}^{+0.02}$  for  $\beta = 0.5$ 

We note that in projection, the lens galaxy is already fully dark-matter dominated inside  $\sim 2.5$  effective radii. For comparison with previous work, we also derive the dark-matter

fraction inside the effective radius and find or  $\beta = 0$ 

$$f_{\rm DM}(< R_{\rm eff}) = 0.60^{+0.15}_{-0.06} \pm 0.1,$$

[68 per cent confidence level (CL)], including a systematic errors of 0.1. The random error is based on the marginalized probability densities shown in Figure 5 and a systematic error is included based on the maximum range of possible dark-matter density slopes. Although the latter is constrained by the models, we extrapolate inward from  $R_{\rm E}$  to  $R_{\rm eff}$ , where this slope could be somewhat different. We note though that the systematic error is rather conservative. The dark-matter fraction increases by  $\sim 0.1$  for  $\beta = 0.5$  and the difference between the Hernquist and Jaffe profiles is negligible (by construction, since they both contain equal fractions of mass inside that radius). This high dark-matter fraction inside the effective radius is consistent with the result found in Auger et al (2010) for SLACS systems.

# 4.3 Stellar Mass Fraction from Stellar Population Constraints

We independently calculate the projected stellar mass fraction inside the Einstein radius, using stellar population synthesis models and the SDSS colors (see Table 1) of the lens galaxy. A comparison between this fraction and that derived from lensing and stellar kinematics provides a direct constraint on the stellar IMF (see also e.g. Treu et al. 2010; Auger et al. 2010).

We use GALAXEV, a library of evolutionary stellar population synthesis models computed using the isochrone synthesis code of Bruzual & Charlot (2003). This code allows one to compute the spectral evolution of stellar populations for a wide range of ages and metallicities. Here we use the 2007 version of GALEXEV kindly provided by S. Charlot (a version commonly known as 'CB07'). We use six Simple Stellar Populations (SSP) models computed with a Salpeter IMF or a Chabrier IMF for a range of metallicities from Z=0.0001 to Z=0.05, all of them with lower mass cutoff of  $M_{\rm low}=0.1\,{\rm M}_{\odot}$  and upper mass cutoff of  $M_{\rm up}=100\,{\rm M}_{\odot}$ . The spectral resolution is 3Å across the wavelength range of 3200–9500Å.

We compute the spectral evolution of the stellar population and the redshift dependence of colors and magnitudes in the SDSS filters  $g,\,r,\,i,$  and z for all SSP models and for a range of ages and star formation histories (SFH). For the SFH model, we use an exponentially declining star formation rate (SFR) with time-scales  $\tau=0.1$  to 0.4 Gyr and as extreme cases an instantaneous burst with  $\tau=0$  or a constant SFR. We compute the redshift evolution of the galaxy colors and magnitudes for a start of star formation between 12 to 5 Gyr, corresponding to a formation redshift of between roughly  $z\sim 5$  and  $\sim 0.5$ . By comparing the model magnitudes to the SDSS magnitudes, we subsequently determine a grid (as function of age, metallically and SFH duration) of likelihood values for each model as well as the total stellar mass. We do this for both the Salpeter and Chabrier IMFs.

We use the standard Bayesian approach, as outlined in Auger et al. (2010), to determine the posterior probability distribution function and the marginalized errors on the total stellar mass of the galaxy, assuming flat priors on all parameters in logarithmic space (e.g. a prior  $\propto 1/\tau$  for  $\tau$ ). The latter assumption is not critical, but given that the

time-scale of the SFH, etc., are unknown a priori, this prior is a better description of our ignorance before making the observations (and modeling). From the resulting cumulative probability function, we calculate the median of the total stellar mass and its 68 per cent confidence interval for both IMFs. Using the observed brightness profile of the galaxy modeled as a Hernquist, Jaffe or deVaucoulers profile (the precise choice is not critical), we determine the fraction of the stellar mass (assuming a constant M/L ratio) within the Einstein radius. The results of this analysis are listed in Table 4, where we report the inferred total stellar mass fraction for each IMF as well as that from lensing and kinematics.

We find that, for the range of assumed luminous profiles and anisotropies for lensing and stellar kinematics, the stellar mass fraction from lensing and stellar kinematics agrees remarkably well with that from stellar population modeling assuming a Salpeter IMF (Fig. 5). This result further supports the results found by Treu et al. (2010) that the IMF of massive early-type lens galaxies is well-matched by an evolved Salpeter IMF.

### 5 BOTTOM-HEAVY IMFS

Recently, van Dokkum & Conroy (2010) have suggested the presence of a large number of stars with masses  $\leq 0.3 M_{\odot}$  in the central regions of early-type galaxies. By measuring the strength of the NaI doublet and the Wing-Ford molecular FeH band in the spectra of eight of the most luminous and massives early-type galaxies in the Virgo and Coma clusters, they infer that the IMF for these systems is steeper than Salpeter, with a slope as steep as  $\alpha = -3$  or even possibly even more 'bottom-heavy' (e.g.,  $\alpha = -3.5$ ). Moreover, a steep IMF also supports the apparently higher number of low mass stars in the Milky Way bulge than in the disk, their IMF does not match the colors and M/L measurements or theoretical arguments for dwarf-deficient IMFs at high redshift.

Here, we investigate this claim by assuming a broken power-law IMF, with the Salpeter slope in the high-mass regime that dominates the SDSS magnitides (i.e. changes in the IMF below this break do not affect the stellar-population analysis carried out above) and a steeper profile in the low-mass range. We test three different values of the break point in the mass function:  $m_{break} = 0.3, 0.5$  and  $0.7\,M_{\odot}$ , respectively. Changing the IMF for stars with  $M \leqslant m_{break}$  does not change the SDSS colors because  $\gtrsim 90$  per cent of the light in the spectral region we studied here is coming from stars with  $M \geqslant 0.7\,M_{\odot}$ . On the other hand, it dramatically changes the total stellar mass of the system, because stars with masses of  $0.1-0.3M_{\odot}$  can contribute at least 60 per cent of the stellar mass for these bottom-heavy IMFs.

We calculate the change in total stellar mass arising from the change in the slope of the IMF:

$$\Delta M = \int_{0.1 M_{\odot}}^{m_{\text{break}}} \left[ \frac{dN}{dm} \Big|_{\text{IMF}} - \frac{dN}{dm} \Big|_{\text{Salp}} \right] m \, dm, \quad (3)$$

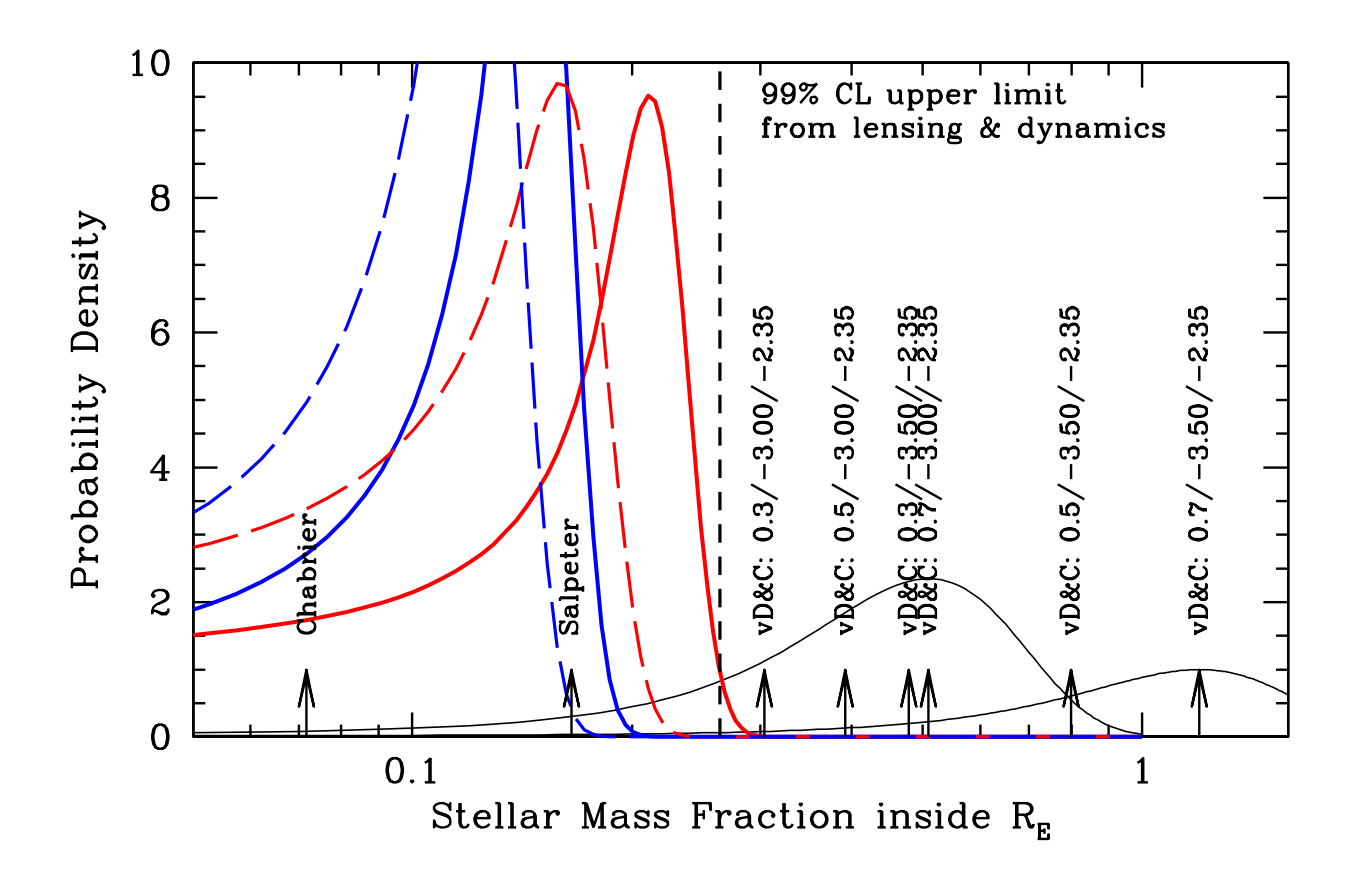


Figure 5. Marginalised PDF for the Hernquist model (red lines) and the Jaffe model (black lines) from lensing and dynamic model. Solid lines are for an anisotropy parameter of  $\beta=0.0$ , and dashed lines for  $\beta=0.5$ . Black arrows show the internal stellar mass fractions with different IMFs from stellar populations analysis. We exclude the Chabrier IMF and the  $\alpha=-3$  IMFs at a confidence level of  $\geqslant 90$  percent and the more bottom-heavy van Dokkum and Conroy ( $\alpha=-3.5$ ) IMFs at a confidence level of 95 percent, while the Salpeter IMF is fully consistent with lensing data.

where

$$\frac{dN}{dm}\Big|_{\text{IMF}} = \begin{cases}
\left(\frac{m}{m_{\text{break}}}\right)^{\beta} & \text{if } m_{\text{break}} < m \leq 100 \,\text{M}_{\odot} \\
\left(\frac{m}{m_{\text{break}}}\right)^{\alpha} & \text{if } 0.1 \,\text{M}_{\odot} < m \leq m_{\text{break}}
\end{cases}$$
(4)

with  $\beta=-2.35$  (Salpeter slope),  $\alpha=-3$  or  $\alpha=-3.5$  for the bottom-heavy IMFS suggested by van Dokkum & Conroy (2010).

Our results for the bottom-heavy stellar mass fraction are listed in Table 4. We also list the likelihood ratios between the nominal isotropic Hernquist model lensing and dynamic stellar mass fraction and the stellar mass fractions obtained from stellar populations and colors for the different IMFs (equivalent to  $\Delta\chi^2$  if the distribution was Gaussian, which we assume as a first approximation), comparing their maximum a poteriori difference with the no-difference hypothesis. Vertical arrows in Figure 5 show the stellar mass fractions predicted by stellar population synthesis models and SDSS color by these different IMFs and the stellar mass fraction obtained with lensing and dynamics. Using

 $m_{\rm break}=0.7M_{\odot}$  and a bottom-heavy IMF, we find that inferred stellar mass fraction exceeds unity for  $\alpha=-3.5$ , inconsistent with the lensing mass. An extreme 'bottom-heavy' IMF with slope of  $\alpha=-3.5$  is inconsistent at the >90 per cent confidence level with the lensing and kinematic results. The  $\alpha=-3$  model is only marginally consistent for  $m_{\rm break}=0.3$  but is also excluded at the >90 per cent confidence level for  $m_{\rm break}=0.7$ . A Salpeter IMF gives the best agreement with the lensing and kinematics. Although other possible explanations, such as a top heavy IMF with more black holes and neutron stars remnants, are still possible.

#### 6 SUMMARY & CONCLUSIONS

In this paper we presented the first results from a new spectroscopic survey of massive early-type lens galaxies: The X-shooter Lens Survey (XLENS). The combination high-fidelity UVIS-IR spectroscopy from the X-Shooter instrument on the VLT, with the strong gravitational lensing mass determination has enabled us to conduct an in-depth study

Table 4. The stellar mass fractions within the Einstein Radius derived from lensing plus stellar kinematics and from stellar population synthesis models, respectively. The likelihood ratio compares maximum a-posteriori difference between the SSP model and the no-difference (null-hypothesis) model with the isotropic Hernquist model, which has the highest inferred stellar mass fraction. The IMF slope is assumed to be  $\alpha = -2.35$  beyond the break  $m_{\text{break}}$  in the mass function. The probabilities in between parentheses are for having a large likelihood ratio of the difference between the two PDFs.

Lensing and Kinematic Model	Anisotropy	Stellar Mass Fraction	
Hernquist	$\beta = 0.0$	$0.19^{+0.04}_{-0.09}$	
	$\beta = 0.5$	$0.13^{+0.04}_{-0.07}$	
Jaffe	$\beta = 0.0$	$0.13^{+0.03}_{-0.05}$	
	$\beta = 0.5$	$0.11^{+0.02}_{-0.05}$	
	$\mathbf{m}_{\mathrm{break}}$		$2\ln(\mathbf{P}_{\max}/\mathbf{P_0})$
Stellar Population Model	$(M_{\odot})$	Stellar Mass Fraction	(HQ versus SSP)
-	$(M_{\odot})$		,
Chabrier	$(M_{\odot})$	$0.07 \pm 0.02$	3.0 (0.08)
Chabrier Salpeter	_ _ _	$0.07 \pm 0.02 \\ 0.17 \pm 0.06$	3.0 (0.08) 0.1 (0.75)
Chabrier Salpeter Bottom-heavy $\alpha = -3.0$	- - 0.3	$0.07 \pm 0.02$ $0.17 \pm 0.06$ $0.30 \pm 0.11$	3.0 (0.08) 0.1 (0.75) 1.0 (0.32)
Chabrier Salpeter Bottom-heavy $\alpha = -3.0$ Bottom-heavy $\alpha = -3.0$	_ _ _	$0.07 \pm 0.02 \\ 0.17 \pm 0.06$	3.0 (0.08) 0.1 (0.75) 1.0 (0.32) 1.9 (0.17)
Chabrier Salpeter Bottom-heavy $\alpha = -3.0$ Bottom-heavy $\alpha = -3.0$ Bottom-heavy $\alpha = -3.0$	- - 0.3 0.5	$0.07 \pm 0.02$ $0.17 \pm 0.06$ $0.30 \pm 0.11$ $0.39 \pm 0.15$	3.0 (0.08) 0.1 (0.75) 1.0 (0.32) 1.9 (0.17) 3.0 (0.08)
Chabrier Salpeter Bottom-heavy $\alpha = -3.0$ Bottom-heavy $\alpha = -3.0$	- 0.3 0.5 0.7	$0.07 \pm 0.02$ $0.17 \pm 0.06$ $0.30 \pm 0.11$ $0.39 \pm 0.15$ $0.51 \pm 0.18$	3.0 (0.08) 0.1 (0.75) 1.0 (0.32) 1.9 (0.17) 3.0 (0.08) 2.8 (0.09)
Chabrier Salpeter Bottom-heavy $\alpha = -3.0$ Bottom-heavy $\alpha = -3.0$ Bottom-heavy $\alpha = -3.0$ Bottom-heavy $\alpha = -3.5$	- 0.3 0.5 0.7	$0.07 \pm 0.02$ $0.17 \pm 0.06$ $0.30 \pm 0.11$ $0.39 \pm 0.15$ $0.51 \pm 0.18$ $0.48 \pm 0.17$	3.0 (0.08) 0.1 (0.75) 1.0 (0.32) 1.9 (0.17) 3.0 (0.08)

of the internal structure of the luminous elliptical galaxy SDSS J1148+1930 at z=0.444. We find the following:

- (i) The luminosity-weighted stellar velocity dispersion is  $\langle \sigma_* \rangle (\lesssim R_{\rm eff}) = 351 \pm 10 \, {\rm km \, s^{-1}}$ , more accurate and considerably lower than a previously published value of  $\sim 450 \, {\rm km \, s^{-1}}$ .
- (ii) A single-component (stellar plus dark) mass model of the lens galaxy yields a logarithmic total-density slope of  $\gamma' = 1.72^{+0.05}_{-0.06}$  (68 per cent CL;  $\rho_{\rm tot} \propto r^{-\gamma'}$ ).
- (iii) The projected stellar mass fraction, derived solely from the lensing and dynamical data, is  $f_*(< R_{\rm E}) = 0.19^{+0.04}_{-0.09}$  (68 per cent CL) inside the Einstein radius for a Hernquist profile and no anisotropy. The dark-matter fraction inside the effective radius  $f_{\rm DM}(< R_{\rm eff}) = 0.60^{+0.15}_{-0.06} \pm 0.1$  (68 per cent CL), where the latter error is systematic.
- (iv) Based on the SDSS colors, we find  $f_{*,\mathrm{Salp}}(< R_{\mathrm{E}}) = 0.17 \pm 0.06$  for a Salpeter IMF and  $f_{*,\mathrm{Chab}}(< R_{\mathrm{E}}) = 0.07 \pm 0.018$  for a Chabrier IMF. A Salpeter IMF gives the best agreement between lensing adn dynamics constraints on the stellar mass fraction, therefore it si preferred over Chabrier. Dwarf-rich IMFs in the lower mass range of 0.1-0.7  $M_{\odot}$ , with  $\alpha \geqslant 3$  (with  $dN/dM \propto M^{-\alpha}$ ) recently suggested by van Dokkum & Conroy for massive early-type galaxies are excluded at the > 90 per cent CL and in some cases violate the total lensing-derived mass limit. Salpeter

This massive early-type galaxy lies at the extreme end of the trend found by, e.g., Auger et al. (2010) that the dark matter fraction within the effective radii is a monotonically increasing function of galaxy mass. In fact SDSS J1148+1930 is already dark-matter dominated in that region. We find that a Salpeter IMF agrees best with the total stellar mass derived from lensing and stellar kinematics, as well as with its SDSS colors. As in Treu et al. (2010)

and Grillo & Gobat (2010), Salpeter seems to be the best option for very massive early-type galaxies. A bottom-light IMF such as Chabrier (or Kroupa) agrees only marginally and we exclude a steep 'dwarf-rich' IMF with  $\alpha=-3.5$  suggested by van Dokkum & Conroy (2010) at >90 per cent CL. Somewhat more shallow IMFs with  $\alpha\approx-3.0$  are marginally acceptable. We conclude that our data are fully consistent with SDSS J1148+1930 being a massive early-type galaxy that is dark-matter dominated inside its effective radius and having a Salpeter IMF. No strong evidence for a bottom-heavy IMF is found, consistent with previous results (Treu et al. 2010).

Further studies are required to break the degeneracy between the central dark-matter fraction and distribution and the stellar IMF. In forthcoming papers of the XLENS survey, we will extend the study to more massive systems at  $z \gtrsim 0.5$  and also a sub-sample of SLACS lenses at  $z \lesssim 0.5$ . Observations are ongoing. In those papers, we will perform more detailed stellar population analyses using the full UVIS-IR spectrum and obtain independent contraints on the the physical parameters that may correlate with IMF normalization (i.e., age and metallicity) or that may be the cause of the correlation between dark-matter and velocity dispersion.

## ACKNOWLEDGMENTS

The use of the Penalized Pixel Fitting developed by Cappellari & Emsellem and of the GALAXEV Software by Bruzual & Charlot are gratefully acknowledged. Data were reduced using EsoRex and XSH pipeline by ESO Data Flow System Group. We thank Prof. P. Groot for instruction on its use. C.S. acknowledges support from an Ubbo Emmius Fellowship. L.V.E.K. is supported in part by an NWO-VIDI pro-

gram subsidy (project number 639.042.505). T.T. acknowledges support from a Packard Research Fellowship.

### REFERENCES

- Arnaboldi M. et al., 1996, ApJ, 472, 145
- Auger M. W., Treu T., Bolton A. S., Gavazzi R., Koopmans L. V. E., Marshall P. J., Moustakas L. A., Burles S., 2010, 2010arXiv1007.2880A
- Auger M. W., Treu T., Gavazzi R., Bolton A. S., Koopmans L. V. E., Marshall P. J., 2010, ApJ, 721L, 163A
- Barnabé M., Czoske O., Koopmans L. V. E., Treu T., Bolton A. S., Gavazzi R., 2009, MNRAS, 399, 21B
- Barnabé M., Koopmans L. V. E., 2007, ApJ, 666, 726B
- Barnabé M., Czoske O., Koopmans L.V. E., Treu T., Bolton A.S., arXiv1102.2261B
- Barnes, J. E. 1992, ApJ, 393, 484
- Baugh C. M., Benson A. J., Cole S., Frenk C. S., Lacey C., 2003, in Bender R., Renzini A., eds, Proc. ESO Workshop, The Mass of Galaxies at Low and High Redshift. Springer, Berlin, p. 91
- Belokurov V., Evans N.W., Moiseev A., King L.J., Hewett P.C., Pettini M., Wyrzykowski L., McMahon R.G., Smith M.C., Gilmore G., Sanchez S.F., Udalski A., Koposov S., Zucker D.B., Walcher C.J., 2007, ApJ, 671, L9
- Bertin G. et al., 1994, A&A, 292, 381
- Binney J. & G.A. Mamon, 1982, MNRAS, 200, 361-375
- Blumenthal G.R., Faber S.M., Primack J.R., Rees M.J., 1984, Nature, 311, 517B
- Bolton, Adam S.; Burles, Scott; Koopmans, Lon V. E.; Treu, Tommaso; Moustakas, Leonidas A., 2006, ApJ, 638, 703B
- Borriello A., Salucci P., Danese L., 2003, MNRAS, 341, 1109
- Brewer B. J., Lewis G. F., 2006, ApJ, 637, 608B
- Brewer B. J., Lewis G. F., 2008, MNRAS, 390, 39B
- Bruzual G., Charlot S., 2003, MNRAS, 344, 1000B
- Bullock J.S., Kolatt T.S., Sigad Y., Somerville R.S., Kravtson A.V., Klypin A.A., Primack J.R., Dekel A., 2001, MN-RAS, 321,598
- Cappellari M., Emsellem E., 2004, PASP 116, 138
- Cappellari, M.; Bacon, R.; Bureau, M.; Damen, M. C.; Davies, Roger L.; de Zeeuw, P. T.; Emsellem, Eric; Falcn-Barroso, Jess; Krajnovi, Davor; Kuntschner, Harald; Mc-Dermid, Richard M.; Peletier, Reynier F.; Sarzi, M.; van den Bosch, Remco C. E.; van de Ven, Glenn, 2006, MN-RAS, 366, 1126
- Carollo C. M., de Zeeuw P. T., van der Marel R. P., Danziger I. J., Qian E. E., 1995, ApJ, 441, L25
- Cole, S., Lacey, C. G., Baugh, C. M., Frenk, C. S. 2000, MNRAS, 319, 168
- Czoske O., Barnabé M., Koopmans L. V. E., Treu T., Bolton A. S., 2008, MNRAS, 384, 987C
- D'Odorico S., Dekker H., Mazzoleni R., Vernet J.,
  Guinouard I., Groot P., Hammer F., Rasmussen P. K.,
  Kaper L., Navarro R., Pallavicini R., Peroux C., Zerbi F.
  M., 2006, Proc.SPIE, 6269, Ground-based and Airborne
  Instrumentation for Astronomy
- Davis M., Efstathiou G., Frenk C.S., White S.D.M., 1985, ApJ,292, 371
- Djorgovski, S., & Davis, M. 1987, ApJ, 313, 59

- Dye S., Evans N.W., Belokurov V., Warren S.J., Hewett P., 2008, MNRAS, 388, 384D
- Dye S., Warren S.J., 2005, ApJ, 623, 31D
- Fabbiano G., 1989, ARA&A, 27, 87
- Faber, S. M., Dressler, A., Davies, R. L., Burstein, D., & Lynden-Bell, D. 1987, Nearly Normal Galaxies. From the Planck Time to the Present, 175
- Falco, E. E., Gorenstein, M. V., & Shapiro, I. I. 1985, ApJ, 289, L1
- Franx M., van Gorkom J. H., de Zeeuw P. T., 1994, ApJ, 436, 642
- Frenk C.S., 1985, Nature, 317, 595F
- Frenk, C. S., White, S. D. M., Davis, M., Efstathiou, G. 1988, ApJ, 327, 507
- Jiang G., Kochanek C.S., 2007, ApJ, 671, 1568J
- Gavazzi R., Treu T., Rhodes J. D., Koopmans L. V. E., Bolton A. S., Burles S., Massey R. J., Moustakas L. A., 2007, ApJ, 667, 176
- Gerhard O.E., 1993, MNRAS, 265, 213G
- Gerhard O., Kronawitter A., Saglia R., Bender R., 2001, AJ, 121, 1936
- Ghigna S., Moore B., Governato F., Lake G., Quinn T., Stadel J., 2000, ApJ, 544,616
- Goldoni P., Royer F., Francois P., Horrobin M., Blanc G., Vernet J., Modigliani A., Larsen J., 2006, in McLean I. S., Iye M., eds, Proc. SPIE Vol. 6269, Ground-based and Airborne Instrumentation for Astronomy. SPIE, Bellingham, p. 62692K
- Graves G.J., Faber S.M., Schiavon R.P., 2009, ApJ, 693,486
   Grillo C., Gobat R., Lombardi M., Rosati P., 2009, A&A, 501, 461
- Grillo C., Gobat R., 2010, MNRAS, 402, L67
- Hernquist L.,1990, ApJ, 356, 359
- Hyde, J. B., & Bernardi, M. 2009, MNRAS, 394, 1978
- Hyde, J. B., & Bernardi, M. 2009, MNRAS, 396, 1171
- Ferreras I., Saha P., Williams L.L.R., Burles S., 2008, AUS, 244, 206F
- Jaffe, W., 1983, MNRAS, 202,995
- Kauffmann G., Charlot S., 1998, MNRAS, 297, L23
- Kochanek, C. S., et al. 2000, ApJ, 543, 131
- Koopmans, L. V. E., & Treu, T. 2002, ApJ, 568L, 5K
- Koopmans, L. V. E., & Treu, T. 2003, ApJ, 583, 606
- Koopmans, L. V. E., Treu, T., Bolton, A. S., Burles, S., & Moustakas, L. A. 2006, ApJ, 649, 599
- Koopmans, L. V. E.; Bolton, A.; Treu, T.; Czoske, O.; Auger, M. W.; Barnab, M.; Vegetti, S.; Gavazzi, R.; Moustakas, L. A.; Burles, S., 2009, ApJ, 703L, 51K
- Loewenstein M., White R. E., 1999, ApJ, 518, 50
- Longhetti M., Saracco P., Severgnini P., Della Ceca R., Braito V., Mannucci F., Bender R., Drory N., Feulner G., Hopp U., 2005, MNRAS, 361, 897L
- Maoz D., Rix H.-W., 1993, ApJ, 416, 425M
- Matsushita K., Makishima K., Ikebe Y., Rokutanda E., Yamasaki N., Ohashi T., 1998, ApJ, 499, L13
- Mould J. R., Oke J. B., de Zeeuw P. T., Nemec J. M., 1990, AJ, 99,1823
- Napolitano N. R., Romanowsky A. J., Tortora C. 2010, MNRAS, 405, 2351
- Quider A.M., Pettini M., Shapley A.E., Steidel C.C, 2009, MNRAS, 398, 1263-1278
- Renzini A., Cimatti A., 1999, in Bunker A. J., van Breugel W. J. M., eds, ASP Conf. Ser. Vol. 193, The HY-Redshift

- Universe: Galaxy Formation and Evolution at High Redshift. Astron. Soc. Pac., San Francisco, p. 312
- Renzini A., 2006, ARA&A, 44, 141R
- Rix H., de Zeeuw P. T., Cretton N., van der Marel R. P., Carollo C. M., 1997, ApJ, 488, 702
- Romanowsky A. J., Douglas N. G., Arnaboldi M., Kuijken K., Merrifield M. R., Napolitano N. R., Capaccioli M., Freeman K. C., 2003, Sci, 301, 1696
- Saglia R. P., Bertin G., Stiavelli M., 1992, ApJ, 384, 433
- Rusin D., Kochanek C.S., 2005, ApJ, 623, 666R
- Rusin D., Ma C., 2001, ApJ, 549L, 33R
- Sánchez-Blázquez P., Peletier R. F., Jiménez-Vicente J., Cardiel N., Cenarro A. J., Falcón-Barroso J., Gorgas, J., Selam, S., Vazdekis A., 2006, MNRAS, 371, 703S
- Seljak U., 2002, MNRAS, 334, 797
- Thomas D., Maraston C., Bender R., Mendes de Oliveira C., 2005, ApJ, 621, 673
- Thomas J., Saglia R.P., Bender R., Thomas D., Gebhardt K., Magorrian J., Corsini E.M., Wegner G., 2007, MN-RAS, 382,657
- Toomre, A. 1977, in Evolution of Galaxies and Stellar Populations, ed. B. M.
- Treu, T., Stiavelli, M., Bertin G., Casertano, C., & Moller, P. 2001, MNRAS, 326, 237
- Treu, T., Stiavelli, M., Casertano, C., Moller, P., & Bertin, G. 1999, MNRAS, 308, 1307
- Treu, T., & Koopmans, L. V. E. 2002, ApJ, 575, 87
- Treu, T., & Koopmans, L. V. E. 2003, AAS, 203, 6801T
- Treu, T., & Koopmans, L. V. E. 2004, ApJ, 611, 739
- Treu, T., Koopmans, L. V. E., Bolton, A. S., Burles, S., & Moustakas, L. A. 2006, ApJ, 650, 1219
- Treu, T., M.W.Auger, Koopmans, R.Gavazzi, P.J.Marshall, A.S.Bolton 2010, ApJ, 709, 1202
- Treu, T., 2010, ARA&A, 48, 87T
- van der Marel R.P., Franx M., 1993, ApJ, 407, 525V
- van der Marel R.P., 1994, MNRAS, 270, 271
- van Dokkum P., Conroy C., 2010, arXiv:1009.5992v1
- van Dokkum P. G., 2001, PASP,113, 1420V
- van Dokkum, P. G., Franx, M., Kelson, D. D., & Illingworth, G. D. 1998, ApJ, 504, L17
- Weijmans A.-M., Krajnovic D., van de Ven G., Oosterloo T. A., Morganti R., de Zeeuw P. T., 2008, MNRAS, 383, 1242
- White, S. D. M., & Frenk, C. S. 1991, ApJ, 379, 52
- White S. D. M., & Rees M., 1978, MNRAS, 183, 341
- Wucknitz, Olaf, 2002, MNRAS, 332, 951W